New global marine gravity model from CryoSat-2 and Jason-1 reveals buried tectonic structure

David T. Sandwell[1]

R. Dietmar Müller[2]

Walter H. F. Smith[3]

Emmanuel Garcia[1]

Richard Francis[4]

1 - Scripps Institution of Oceanography, La Jolla, CA, 92093, USA
2 - School of Geosciences, The University of Sydney, New South Wales, Australia.
3 - NOAA Laboratory for Satellite Altimetry, College Park, MD, 20740, USA
4 – ESA/ESTEC, Keplerlaan 1, 2201AZ Noordwijk, The Netherlands

Revised for Science, August 20, 2014

Abstract

Gravity models are powerful tools for mapping tectonic structures, especially in the deep ocean basins where the topography remains unmapped by ships or is buried by thick sediment. We combine new radar altimeter measurements from CryoSat-2 and Jason-1 with existing data to construct a global marine gravity model two times more accurate than previous models. We find an extinct spreading ridge in the Gulf of Mexico, a major propagating rift in the South Atlantic Ocean, abyssal hill fabric on slow spreading ridges, and thousands of previously uncharted seamounts. These discoveries allow us to understand regional tectonic processes and highlight the importance of satellite-derived gravity models as one of the primary tools for the investigation of remote ocean basins.

Fracture zones (FZs) spanning the ocean basins reveal the breakup of the continents and the geometry of seafloor spreading *(1)*. The exact intersection points of the FZs along conjugate continental margins are used for precise reconstruction of the continents *(2-4)*. These FZ intersections are commonly buried by several kilometers of sediments that flow off the continents to fill the voids created by the thermal subsidence of the rifted margins *(5)*. This sediment cover extends hundreds to thousands of kilometers out onto the oceanic lithosphere resulting in a relatively flat and featureless seafloor. Reflection seismic profiles can reveal the underlying basement topography of the fracture zones but the data coverage is usually insufficient to map out the intersections. In areas of thin sediment cover, the topographic ridges and troughs along the fracture zones produce large gravity anomalies that are easily traced across the ocean basins (Fig. 1). However, when the topography becomes buried by sediment the original density contrast of the seafloor topography is reduced resulting in more subdued, and sometimes sign reversed, gravity signatures *(6)*. Moreover, as the lithosphere ages and cools the seafloor subsides, causing a blurring of the gravity anomalies; smaller wavelengths of the gravity field become less well resolved with increasing water depth. Previous global marine gravity models derived from satellite altimetry had sufficient accuracy and coverage to map all fracture zones in unsedimented seafloor *(7)*, but the 3-5 mGal of gravity noise blurred the small signatures of sediment-covered topography such as seamounts and fracture zones. Here we report on a new global marine gravity model having ~2 mGal accuracy that is providing a dramatically improved resolution of the 80% of the seafloor that remains uncharted or is buried beneath thick sediment.

Gravity field accuracy derived from satellite altimetry depends on three factors: altimeter range precision, spatial track density, and diverse track orientation. Recently two altimeter data sets with high track density have become available (CryoSat-2, and Jason-1) to augment the older altimeter data (Geosat, and ERS-1) resulting in a factor of 2-4 improvement in the global marine gravity field. Their newer radar technology results in a 1.25 times improvement in range precision that maps directly into gravity field improvement *(8)*. The new altimeters also contribute more than 70 months of data compared with the 31 months provided by the older satellites. CryoSat-2 has provided the most dense track coverage because, while it has a nominal 369-day repeat orbit period, the ground tracks are allowed to drift within a 5 km band so after 4 years in orbit it has provided a nominal track spacing of about 2.5 km. Jason-1 provided 14 months of dense track coverage during its geodetic phase resulting in a track spacing of 7.5 km.

Most of the improvement in the altimeter-derived gravity field occurs in the 12 to 40 km wavelength band, which is of interest for investigation of structures as small as 6 km. The current version of the altimeter-derived gravity field has an accuracy about 2 mGal *(8)*. Unlike terrestrial gravity where coverage is uneven, these accuracies are available over all marine areas and large inland bodies of water so this gravity provides an important tool for exploring the deep ocean basins. At scales smaller than 200 km, variations in marine gravity primarily reflect seafloor topography generated by plate tectonics such as ridges, FZs, and abyssal hills. Many FZs can now be traced much more closely to the continental margins, and one can also better interpret buried migrating, unstable FZs, which has the potential to improve the use of fracture zones as tie points for reconstructions of the boundaries between continental fit reconstructions (Fig. 1). In addition to fracture zones there are other tectonic features associated with continental margins, such as the boundaries between continental and oceanic crust (COB), that can now be mapped in greater detail.

The first example (Fig. 2) is in the Gulf of Mexico where thick sediments obscure the fracture zones and extinct ridges. Reconstruction models provide the overall framework of counterclockwise rotation of the Yucatan plate with respect to North America as well as a generalized position for the COB *(9)*. The new vertical gravity gradient images confirm and refine the positions of these tectonic boundaries. Extinct spreading ridges produce a negative gravity signature because the relatively high-density sediment cover largely cancels the positive gravity effect of the topographic ridge leaving the negative gravity signature of the compensating Moho topography *(6)*. In this region the Moho is more than 15 km beneath the sea surface so the effects of upward continuation reduce and smooth the anomaly.

The second example is on the African ridge flank where the new data reveal a major tectonic feature that was not visible in previous satellite gravity data sets due to high-frequency noise. The newly discovered feature is a set of tectonic lineaments roughly between 8°S and 12°S striking northwest-southeast and obliquely dissected by individual en-echelon faults, stretching from the Bodo Verde

Fracture Zone in the north into the middle of the Cretaceous Magnetic Quiet Zone at its southeastern extension (Fig. 1b). This feature is about 800 km long and 100 km wide, and does not follow either the azimuth of nearby seafloor isochrons or fracture zones. A reconstruction of this feature at magnetic chron 34 (83.5 Ma) (Fig. 3) reveals that it has a mirror-image counterpart on the South American plate, but this conjugate feature is represented only by a relatively faint gravity lineament (Fig. 3). This feature visible in the filtered vertical gravity gradient image, marking a boundary between swaths of differently textured seafloor fabric to the east and west of the lineament (Fig. 3). The geometry of the two features suggests that they form a pair of an extinct ridge (on the African side) and a pseudofault (on the South American side), created by a northward ridge propagation episode between ~100 and 83 Ma. An absolute hotspot-based plate reconstruction using the rotation parameters from *O'Neill et al*. *(10)* indicates that the Cardno hotspot (Fig. 3) may have been situated not far north of the northern tip of the ridge propagator, where it abuts the Bodo Verde Fracture Zone; this is where the propagator came to a halt. These observations conform with the inference that ridges have a tendency to propagate towards hotspots/plumes and that propagation events and resulting spreading asymmetries are frequently contained within individual spreading corridors bounded by fracture zones *(11)*. The existence of major previously unknown ridge propagation events will also be relevant for interpreting marine magnetic anomaly sequences during the Cretaceous Normal Superchron on conjugate ridge flanks *(12)*.

One of the most important uses of this new marine gravity field will be to improve the estimates of seafloor depth in the 80% of the oceans having no depth soundings. The most accurate method of mapping seafloor depth uses a multibeam echosounder mounted on a large research vessel. However even after 40 years of mapping by hundreds of ships one finds that more than 50% of the ocean floor is more than 10 km away from a depth measurement. Between the soundings the seafloor depth is estimated from marine gravity measurements from satellite altimetry *(13)*. This method works best on seafloor where sediments are thin resulting in a high correlation between seafloor topography and gravity anomaly in the 12 km to 160 km wavelength band. The shorter wavelengths are attenuated because of Newton's inverse square law while the longer wavelengths are partially cancelled by the gravity anomalies caused by the isostatic topography on the Moho *(13)*. The abyssal hill fabric created during the seafloor spreading process has characteristic wavelengths of 2-12 km so it is now becoming visible in the VGG models especially on the flanks of the slower spreading ridges *(14)*. Additionally, seamounts between 1 and 2 km tall, that were not apparent in the older gravity models, are becoming visible in the new data. As CryoSat-2 continues to map the ocean surface topography, the noise in the global marine gravity field will decrease. Additional analysis of the existing data, combined with this steady decrease in noise will enable dramatic improvements in our understanding of deep ocean tectonic processes.

References

1. Wilson, J.T. (1965) A New Class of Faults and Their Bearing on Continental Drift. *Nature* 207:343-347.
2. Cande, S., J. LaBrecque, & W. Haxby (1988) Plate kinematics of the South Atlantic: Chron C34 to present. *Journal of Geophysical Research: Solid Earth* 93(B11):13479-13492.
3. Heine, C., J. Zoethout, & R. D. Müller (2013) Kinematics of the South Atlantic rift. *Solid Earth* 4(2).
4. Lawver, L.A., L. M. Gahagan, & I. W. Dalziel (1998) A tight fit-Early Mesozoic Gondwana, a plate reconstruction perspective. *Memoirs of National Institute of Polar Research. Special issue*, Vol 53, pp 214-229.
5. Steckler, M.S. & A. B. Watts (1978) Subsidence of the Atlantic-type continental margin off New York. *Earth and Planetary Science Letters* 41:1-13.
6. Liu , C. S., D. T. Sandwell, and J. R. Curray, The Negative Gravity Field Over the 85°E Ridge, J. Geophys. Res., 87, 7673-7686, 1982.
7. Matthews, K., R. D. Müller, P. Wessel, & J. M. Whittaker (2011) The tectonic fabric of the ocean basins. *Journal of Geophysical Research: Solid Earth* 116(B12109):1-28.
8. Materials and methods are available as supplementary material on Science Online.

9. Pindell, J. and L. Kennen, Tectonic evolution of the Gulf of Mexico, Caribbean and northern South America in the mantle reference frame: an update (2009), In: James, K., Lorente, M. A. & Pindell, J. (eds) The geology and evolution of the region between North and South America, Geological Society of London, Special Publication.

10. O'Neill, C., R. D. Müller, & B. Steinberger (2005) On the uncertainties in hot spot reconstructions and the significance of moving hot spot reference frames. *Geochem. Geophys. Geosyst.* 6(4):Q04003.

11. Müller, R.D., W. R. Roest, & J. Y. Royer (1998) Asymmetric sea-floor spreading caused by ridge-plume interactions. *Nature* 396(6710):455-459.

12. Granot, R., J. Dyment, & Y. Gallet (2012) Geomagnetic field variability during the Cretaceous Normal Superchron. *Nature Geoscience* 5(3):220-223.

13. Smith, W.H.F. and D.T. Sandwell, 1997: Global seafloor topography from satellite altimetry and ship depth soundings: evidence for stochastic reheating of the oceanic lithosphere, *Science,* 277, 1956-1962.

14. Goff, J. A., W. H. F. Smith, K. A. Marks, (2003) The Contributions of Abyssal Hill Morphology and Noise to Altimetric Gravity Fabric, *Oceanography, 17*, 24-37.

15. Pavlis, N. K., S. A. Holmes, S. C. Kenyon, and J. K. Factor (2012), The development and evaluation of the Earth Gravitational Model 2008 (EGM2008), J. Geophys. Res., 117, B04406, doi:10.1029/2011JB008916.

16. Seton, M., et al. (2012), Global continental and ocean basin reconstructions since 200 Ma, Earth-Science Reviews, 113, 212-270.

17. Mohriak, W., M. Nóbrega, M. Odegard, B. Gomes, & W. Dickson (2010) Geological and geophysical interpretation of the Rio Grande Rise, south-eastern Brazilian margin: extensional tectonics and rifting of continental and oceanic crusts. *Petroleum Geoscience* 16(3):231-245.

18. Scotchman, I., G. Gilchrist, N. Kusznir, A. Roberts, & R. Fletcher (2010) The breakup of the South Atlantic Ocean: formation of failed spreading axes and blocks of thinned continental crust in the Santos Basin, Brazil and its consequences for petroleum system development. *Geological Society, London, Petroleum Geology Conference series*, (Geological Society of London), pp 855-866.

19. Mohriak, W.U., P. Szatmari, & S. Anjos (2012) Salt: geology and tectonics of selected Brazilian basins in their global context. *Geological Society, London, Special Publications*), Vol 363, pp 131-158.

20. Chandler, M.T. & P. Wessel (2008) Improving the quality of marine geophysical track line data: Along‐track analysis. *Journal of Geophysical Research: Solid Earth* 113(B2).

21. Andersen, O.B. & P. Knudsen (1998) Global marine gravity field from the ERS‐1 and Geosat geodetic mission altimetry. *Journal of Geophysical Research: Oceans* 103(C4):8129-8137.

22. Haxby, W., G. Karner, J. LaBrecque, & J. Weissel (1983) Digital images of combined oceanic and continental data sets and their use in tectonic studies. *Eos, Transactions American Geophysical Union* 64(52):995-1004.

23. Hwang, C. & B. Parsons (1996) An optimal procedure for deriving marine gravity from multi-satellite altimetry. *Geophysical Journal International* 125(3):705-718.

24. Sandwell, D.T. & W. H. F. Smith (2009) Global marine gravity from retracked Geosat and ERS-1 altimetry: Ridge segmentation versus spreading rate. *Journal of Geophysical Research: Solid Earth* 114(B1):B01411.

25. Sandwell, D.*, et al.* (2013) Toward 1-mGal accuracy in global marine gravity from CryoSat-2, Envisat, and Jason-1. *The Leading Edge* 32(8):892-899.

26. Garcia, E.S., D. T. Sandwell, & W. H. F. Smith (2014) Retracking CryoSat-2, Envisat and Jason-1 radar altimetry waveforms for improved gravity field recovery. *Geophysical Journal International*:ggt469.

27. Wingham, D. J., R. Francis, S. Baker, C. Bouzinac, R. Cullen, P. de Chateau-Thierry, S. Laxon, U. Mallow, C. Mavrocordatos, L. Phalippou, G. Ratier, L. Rey, F. Rostan, P. Viau and D. Wallis, CryoSat: a mission to determine fluctuations in Earth's land and marine ice fields, (2006) *Adv. Space Res.* 37:841–871.

28. Griffiths, H.D. (1988) Synthetic Aperture Processing for Full-Deramp Radar Altimeters, *Electronic Lett.*, 24, 371 - 373.

29. Johnson, W. T. K. (1991) Magellan Imaging Radar Mission to Venus, *Proc. IEEE*, Vol. 79, No. 6.

30. Raney, R. K. (1998) The delay Doppler radar altimeter, *IEEE Trans Geosci. Remote Sens.* 36(5):1578–1588.

31. Phalippou, L. and V. Enjolras (2007) Re-tracking of SAR altimeter ocean power waveforms and related accuracies of sea surface height, significant wave height, and wind speed, *Proc. IEEE IGARSS*, Barcelona.

32. Weickert, J. (1999) Coherence-enhancing diffusion of colour images. *Image and Vision Computing* 17(3):201-212.

33. Fehmers, G.C. & C. F. Höcker (2003) Fast structural interpretation with structure-oriented filtering. *Geophysics* 68(4):1286-1293.

Acknowledgements
The CryoSat-2 data were provided by the European Space Agency, and NASA/CNES provided data from the Jason-1 altimeter. This research was supported by the National Science Foundation (OCE-1128801), the Office of Naval Research (N00014-12-1-0111), the National Geospatial-Intelligence Agency (HM0177-13-1-0008) and ConocoPhillips. Version 23 of global grids of gravity anomaly and VGG can be downloaded from the supplementary materials and also at the following ftp site ftp://topex.ucsd.edu/pub/global_grav_1min. The manuscript contents are the opinions of the authors and the participation of W.H.F. Smith should not be construed as indicating that the contents of the paper are a statement of official policy, decision, or position on behalf of NOAA or the U. S. Government.

Fig. 1. Ocean gravity maps. (a) New marine gravity anomaly map derived from satellite altimetry reveals tectonic structures of the ocean basins in unprecedented detail, especially in areas covered by thick sediments. Land areas show gravity anomaly from EGM2008 *(15)*. (b) Vertical gravity gradient (VGG) map derived from satellite altimetry highlights fracture zones crossing the South Atlantic Ocean basin (e.g. yellow line). Areas outlined in red are small amplitude anomalies in areas where thick sediment has diminished the gravity signal of the basement topography. The full resolution gravity anomaly and vertical gravity gradient models can be viewed in Google Earth using the following files:
(ftp://topex.ucsd.edu/pub/global_grav_1min/global_grav.kmz)
(ftp://topex.ucsd.edu/pub/global_grav_1min/global_grav_gradient.kmz).
The grids are available in the supplementary material as well as at the following ftp site (ftp://topex.ucsd.edu/pub/global_grav_1min).

Fig. 2. Gulf of Mexico vertical gravity gradient (VGG). (a) Uninterpreted (b) Our interpretation of tectonic structures, after *Pindell and Kennan* (10). VGG reveals subtle signatures of the extinct spreading ridges and fracture zones as well as a significant change in amplitude across the boundary between continental and oceanic crust (COB). Mercator projection, grey scale saturates at +/- 20 eotvos units.

Fig. 3. South Atlantic filtered VGG. Reconstructed at chron 34 (83.5 Ma, orthographic projection) with Africa fixed *(16)*. Major tectonic and volcanic seafloor features and offshore sedimentary basins are labeled. The mid-ocean ridge is outlined in red, the extinct Abimael spreading ridge is shown as red dashed line and the reconstructed position of the Cardno hotspot (CS) is outlined by a red star. Most of the seafloor shown in this reconstruction was formed during the Cretaceous Normal Superchron. Also note the extinct Abimael spreading ridge between the Santos Basin and Sao Paulo Plateau offshore Brazil is now visible as a negative VGG anomaly (dashed red line) as compared to previous interpretations *(17, 18)*. This region is of great interest for oil and gas exploration as it is one of the most extensive deep water oil and gas frontiers globally, with several recent discoveries *(19)*.

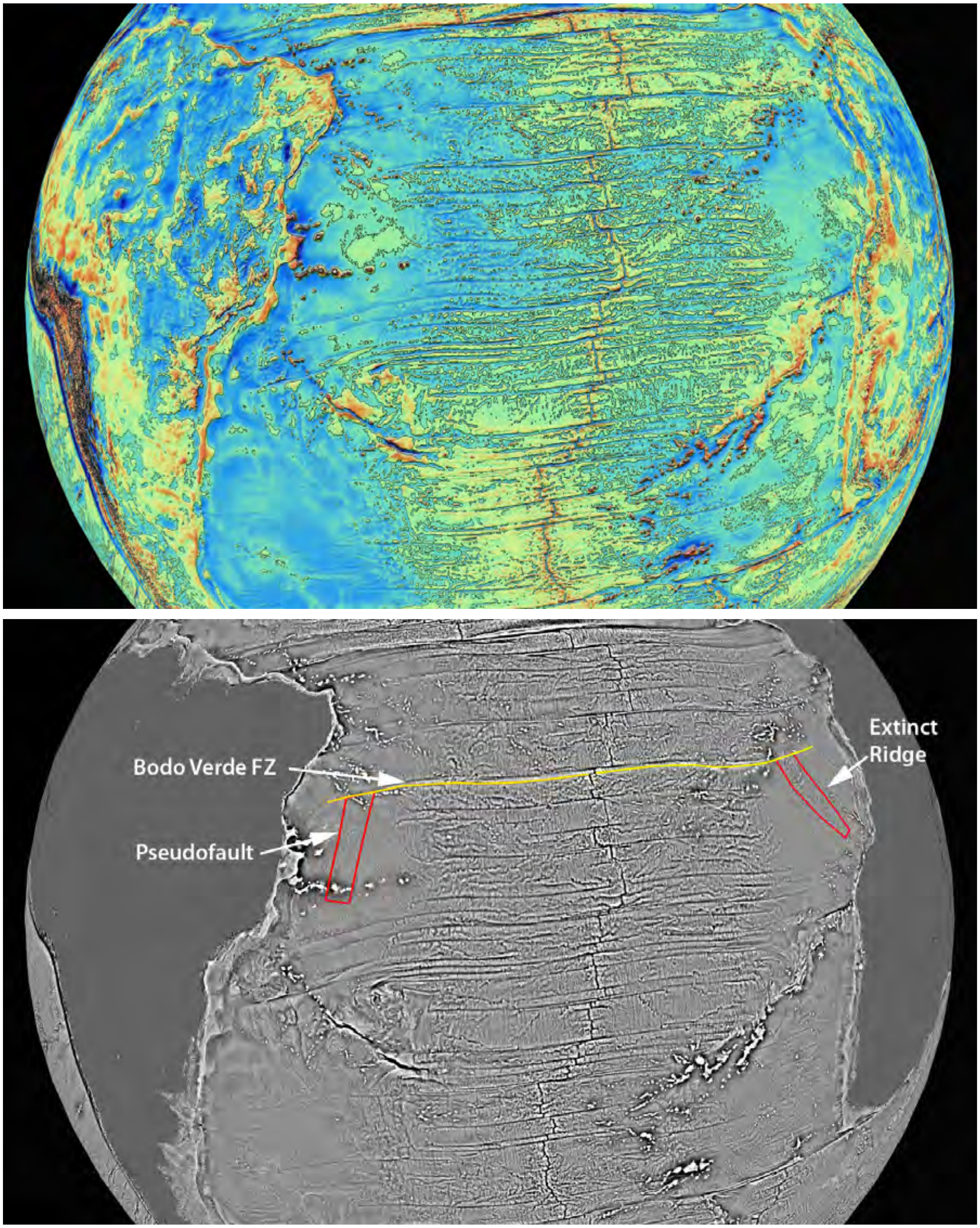
Extinct
Ridge
Bodo Verde FZ
Pseudofault

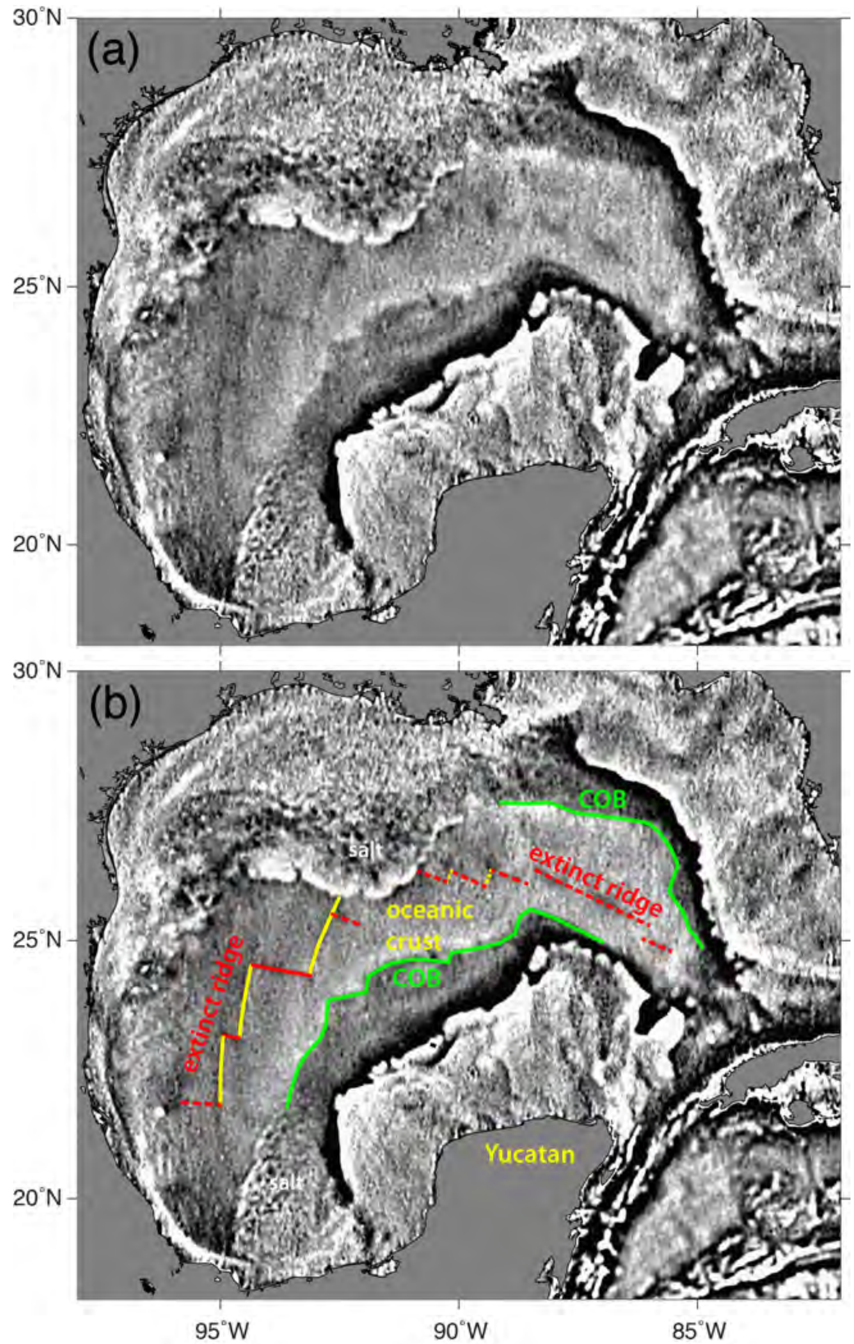

30°N
(a)
25°N
20°N
30°N
(b)
COB
salt
extinct ridge
oceanic
crust
25°N
extinct ridge
COB
Yucatan
salt
20°N
95°W
90°W
85°W

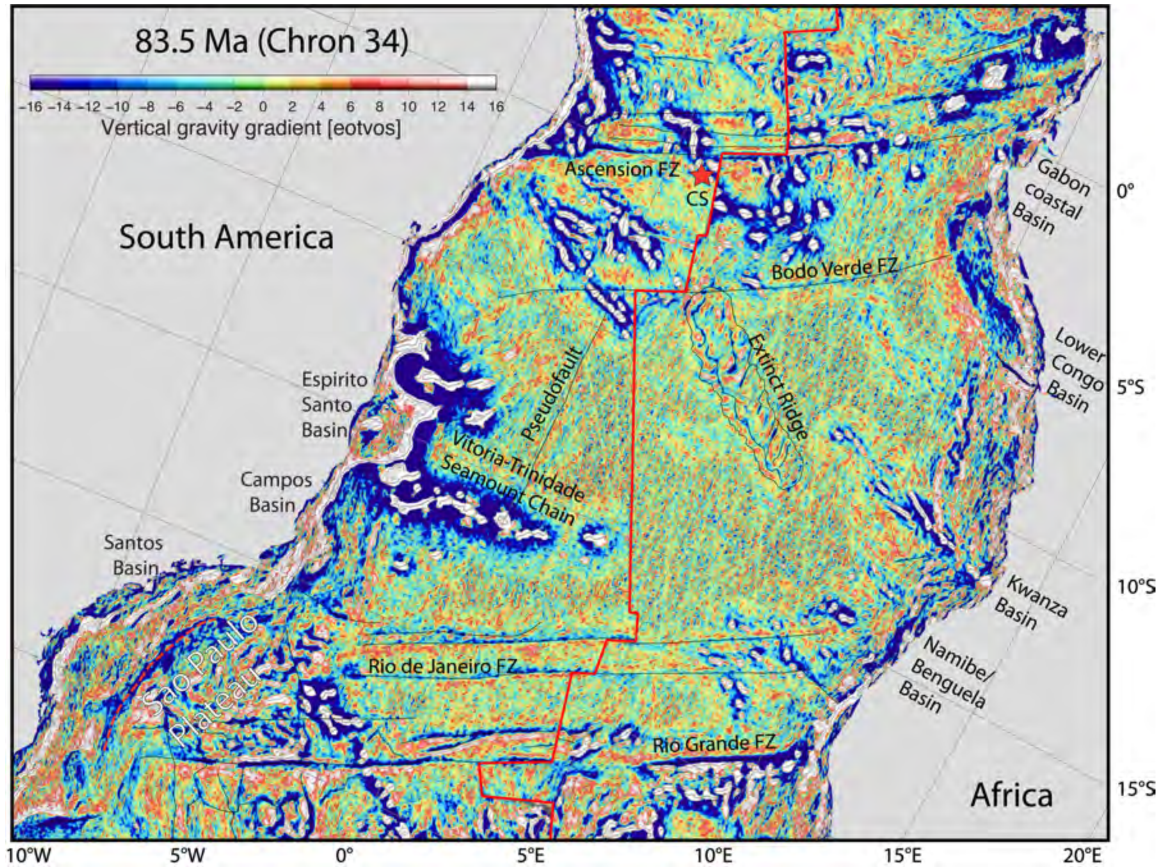
83.5 Ma (Chron 34)
-16 -14 -12 -10 -8 -6 -4 -2 0 2 4 6 8 10 12 14 16
Vertical gravity gradient [eotvos]
South America
Africa
Ascension FZ
CS
Gabon coastal Basin
Bodo Verde FZ
Lower Congo Basin
Espirito Santo Basin
Pseudofault
Extinct Ridge
Vitoria-Trinidade Seamount Chain
Campos Basin
Santos Basin
Kwanza Basin
Namibe/ Benguela Basin
Sao Paulo Plateau
Rio de Janeiro FZ
Rio Grande FZ
0°
5°S
10°S
15°S
10°W
5°W
0°
5°E
10°E
15°E
20°E